Water Practice & Technology

IWA PUBLISHING

Water Practice & Technology Vol 18 No 10, 2341 doi: 10.2166/wpt.2023.156

Sol–gel catalysts immobilized on stainless steel meshes for Ba^{2+} removal in a continuous flow process: An experimental design

Lisandra N. Bueno[a], Michel Zampieri Fidelis[b], Eduardo Abreu[b], Angelo Marcelo Tusset[c] and Giane Gonçalves Lenzi[a,*]

[a] Department of Chemical Engineering, University of Technology, Ponta Grossa, PR, Brazil
[b] Department of Chemical Engineering, State University of Maringa, Maringa, PR, Brazil
[c] Department of Industrial Engineering, Federal University of Technology, PR, Brazil
*Corresponding author. E-mail: gianeg@utfpr.edu.br

GG, 0000-0003-2065-9622

ABSTRACT

This study describes the use of a continuous flow system for photocatalytic reactions employing a TiO_2 sol–gel structured catalyst. The catalyst was immobilized on various stainless steel meshes to investigate the barium(II) removal. To verify its photocatalytic activity, batch tests were carried out and the results were compared to the commercial catalyst P25. Effects of thermal treatment on the structured catalyst were investigated. The continuous flow photocatalytic tests were conducted under different experimental conditions through an experimental design to verify the effect of the parameters (pH and volume flow). The results of the batch tests indicated that the TiO_2 sol–gel catalyst showed very similar activity to the TiO_2 P25 when used in powder suspension (32% reduction of Ba^{2+}). In the continuous flow process, maximum adhesion of catalysts on meshes was found at a calcination temperature of 623 K. The experimental design indicated the pH as a significant parameter in the studied conditions. It was observed that at pH levels close to 7, also indicated by the study of the zero charge point and lower flow rates, it was possible to obtain ~20% removal of Ba^{2+} ions, in a continuous flow reactor with a residence time of 83 min.

Key words: heavy metals, photocatalysis, stainless steel meshes, TiO_2

HIGHLIGHTS

- Study for the application of photocatalytic processes for industrial decontamination.
- Synthesis of sol-gel catalysts structured on stainless steel meshes.
- Application of a continuous flow process to remove industrial pollutants.
- Removal of barium(II) from surface waters
- Effect of pH and calcination temperature on immobilized catalysts applied to barium(II) removal.

GRAPHICAL ABSTRACT

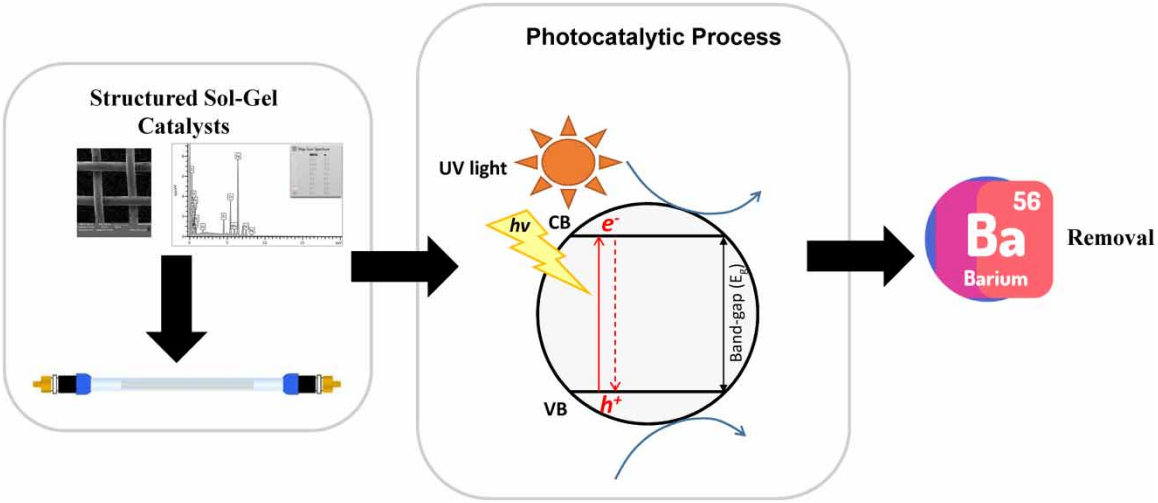

1. INTRODUCTION

The need to increase the production of food and industrial inputs, in order to serve the market, has generated waste and an increase in the pollutant load in water, air, and soil. In this polluting load are organic compounds (emerging pollutants and industrial plants) (Khadim *et al.* 2022) and inorganic compounds (heavy metals) (Jabbar *et al.* 2022).

Barium is present in effluents from chemical, petrochemical, automotive, and metallurgical industries, among others. In addition to effluents, groundwater is also susceptible to contamination by this metal, due to some urban activities such as domestic slurry production, septic tanks, leaking municipal sewage networks, and leaking gas stations. Also, agricultural activities, in general, by the inadequate use of mineral and organic fertilizers, herbicides, and pesticides, cause metal contamination. However, there are few studies in the literature concerned with the Ba pollution potential. However, due to the new and growing barium applications in industrial processes and its consequent increase in human exposure, there is a need to develop effective processes for the removal of barium(II) from the environment (Pepe *et al.* 2013; Kravchenko *et al.* 2014; Zhao *et al.* 2022).

In this context, many methods have been studied to remove contaminating compounds, for example, adsorption (Atiyah *et al.* 2022; Khadim *et al.* 2022), ozonation (Graça *et al.* 2020), photocatalysis (Fidelis *et al.* 2019; Abbood *et al.* 2023), photocatalytic ozonation (Fidelis *et al.* 2023), UV (Bueno *et al.* 2023), UV/TiO_2, electrochemical processing (Kadhum *et al.* 2021), Fenton (Ali *et al.* 2023), and UV/H_2O_2 process (Ali *et al.* 2022b).

In particular, the photocatalytic process has attracted a lot of attention due to efficient contaminant removal. However, application of photocatalysts usually occurs in suspension, which guarantees a large surface area for the reaction and facilitates a mass transfer process (Fontana *et al.* 2018; Abreu *et al.* 2021). The use of photocatalysts in suspension, especially in continuous flow processes, requires a subsequent separation process to remove the catalyst from the final effluent. Nevertheless, most semiconductors are fine powders, requiring additional procedures for their recovery. In this way, the cost of the process increases, making its application on an industrial scale unfeasible. Thus, there is a need for the development of catalysts that can be easily recovered and reused.

The use of immobilized catalysts can reduce costs and simplify the process. Many attempts to immobilize TiO_2 photocatalyst on different support structures were made. These studies sought to increase the surface/volume ratio at the same time, which consequently increases the photocatalytic activity. Materials being studied include encapsulated (Atiyah *et al.* 2022), biopolymer (Lenzi *et al.* 2022), magnetic (Oliveira *et al.* 2023), among others. Some of these materials can be affected by process parameters such as pH, temperature, and contaminant concentration.

Semiconductors can be immobilized on different materials to form mechanically resistant layers (Rachel *et al.* 2002; Miranda-García *et al.* 2010; Shan *et al.* 2010; Panniello *et al.* 2012; Bet-moushoul *et al.* 2016; Manassero *et al.* 2017; Cunha *et al.* 2018; Karaolia *et al.* 2018). Although many studies point out that catalytic systems with immobilized catalyst are less efficient, some authors such as Gar Alalm *et al.* (2016), Vaez *et al.* (2012), Zhang

et al. (2017), and Adamek *et al.* (2019) achieved greater catalytic activity for catalysts on a suitable support, compared to suspended catalysts.

El-Kalliny *et al.* (2014) used TiO_2 immobilized on stainless steel meshes for water purification. The study indicated that stainless steel wire was a good photocatalyst substrate due to its large surface area and the possibility for light to be effectively distributed through it.

Thus, the contribution of the manuscript was the synthesis of TiO_2 structured catalysts using a sol–gel method and immobilizing them on stainless steel meshes. These catalysts were applied in barium removal, in a continuous system. To better evaluate the process, a study of parameters involved in the process was carried out through the experimental design. The catalyst was characterized by scanning electron microscopy (SEM) and point-of-zero charge (PZC).

2. EXPERIMENTAL PROCEDURE

Figure 1 shows a schematic diagram of the process that includes catalyst synthesis, immobilization on meshes, thermal treatment, and removal of Ba^{2+}.

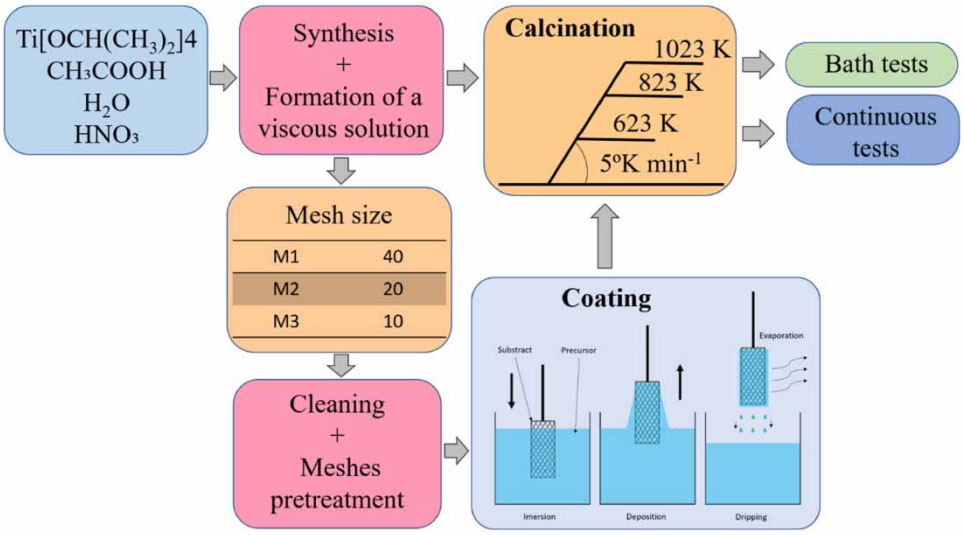

Figure 1 | Schematic diagram of the process.

2.1. Catalyst synthesis

2.1.1. Chemicals

The following chemicals were used in the experiments: glacial acetic acid (Neon); titanium(IV) isopropoxide 97% (Aldrich); nitric acid PA 65% (Synth); absolute ethanol PA (Dinâmica); barium nitrate PA (Perquim); formic acid 0.5 g/L (Synth); and TiO_2 P25 (Degussa).

2.1.2. TiO_2 sol–gel

The synthesis of the sol–gel TiO_2 precursor solution started with the addition of 10 mL of glacial acetic acid to an Erlenmeyer flask that is stirred using a magnetic stirrer, followed by the addition of 50 mL of titanium(IV) isopropoxide, kept under stirring for 5 min. Then, 200 mL of deionized water was added dropwise, keeping the solution stirred for 1 h. Subsequently, 6 mL of nitric acid was added to the solution, which was kept under stirring for 12 h at room temperature. After this period, it was submitted to the evaporation process in order to reach a more viscous consistency that provides a better adhesion to the support (Denisov *et al.* 2017; Martino 2022).

2.1.3. Catalyst immobilization

The TiO_2 catalyst synthesized by the sol–gel method was immobilized on 304 stainless steel nets in three different mesh sizes as shown in Table 1.

Table 1 | Names and characteristics of stainless steel nets

	Mesh size	Wire diameter (mm)	Mesh hole (mm)	Hole area (%)
M1	40	0.23	0.41	41
M2	20	0.36	0.91	51
M3	12	0.71	1.40	44

The stainless steel nets were previously cut into a rectangle shape of 20 × 4 cm, and then turned into a cylindrical shape. The nets were washed and dried at 343 K for 2 h in an oven with air circulation and renewal. The coating process was started using the wash-coating method, the nets were dipped in the precursor solution for 1 min and left to dry at room temperature. After the drying period, the nets were calcined in a heating ramp at 623, 823, and 1,023 K at a rate of 3.2 K min^{-1}. Then, the structured catalyst was cooled to room temperature by washing under running water, and then sonicated for 15 min in order to remove excess semiconductors. Subsequently, the nets were again dried at 343 K for 2 h.

2.1.4. Characterization

The powder catalyst was characterized by: (*i*) PZC determination. The PZC was determined by applying a batch equilibration experiment (Guilarduci *et al.* 2006). In Erlenmyer flasks, 50 mg of catalyst and 50 ml of ultrapure water were mixed, under different initial pH values. Followed by constant stirring for 24 h in a shaker at 298 K and 120 rpm. The final pH measurements of the suspensions were performed. The pH_{PZC} corresponds to the average of the final pH values which tended to be a constant value, regardless of the initial pH value. (*ii*) SEM associated with energy dispersive spectroscopy (EDS): SEM characterization was performed using a VEJA 3 LMU – TESCAN microscope with a 30 kV filament, 3.0-nm resolution SE, and retractable BSE (higher energy electrons) detectors, low-vacuum mode (500 Pa), chamber with 230 mm of inner diameter, and CCD camera for preview of samples. The microscope is also equipped with an EDS detector, model AZTec Energy X-Act, resolution of 130 eV, brand Oxford. Before performing the analyses, all catalysts were metallized with gold for 10 min using the IC-50 ION COATER-SHIMADZU equipment.

2.2. Photocatalytic tests

2.2.1. Batch experiments

Batch tests were carried out with the TiO_2 sol–gel catalyst powder (obtained by the synthetized sol–gel viscous solution drying and its calcination at 823 K) in suspension, in order to verify the photocatalytic activity of the TiO_2 sol–gel catalyst. The barium synthetic solution was made using barium nitrate in order to get a solution concentration of 50 mg/L. Then, formic acid was added in the solution at the rate of 0.5 g/L followed by the addition of 0.5 g/L of powdered catalyst. Also, tests with commercial TiO_2 P25 were carried out in order to compare both catalysts. The duration of photocatalytic reactions was 90 min, where samples should be collected every 15 min. The glass reactor used had a 600 mL of capacity, with constant temperature (293 K), magnetic stirring, and air flow at a rate of 5 cm^3/min. The radiation was provided by a 125-W and 10-mW/cm^2 irradiance mercury vapor lamp, which had its original protective bulb removed to avoid interference. The concentration of barium(II) present in the samples was measured using Atomic Absorption Spectrometry – Perkin Elmer, model AAnalyst 700 equipped with an FIAS 100 hydride generation system. The barium(II) removal percentage was obtained by the following equation:

$$\text{Barium (II) removal rate } \% = \frac{C_0 - C_f}{C_0} \tag{1}$$

where C_0 represents the initial barium(II) concentration and C_f represents the final barium(II) concentration.

The calibration curve was performed with Ba^{2+} at the following concentrations: 5, 10, 15, 20, 25, 30, 40, and 50 ppm. The correlation coefficient obtained was 0.998.

2.2.2. Continuous flow experiments

The continuous flow reactor used to carry out the experiment was a PTC type (parabolic concentrator reactor). The photoreactor tube is made of borosilicate glass, a material that provides a high UV transmission (90%) and is

shown in Figure 2(a). The glass tube dimensions include an external diameter of 20 mm, internal diameter of 16 mm, and length of 392 mm. The system used to perform the photocatalytic tests is represented in Figure 2(b).

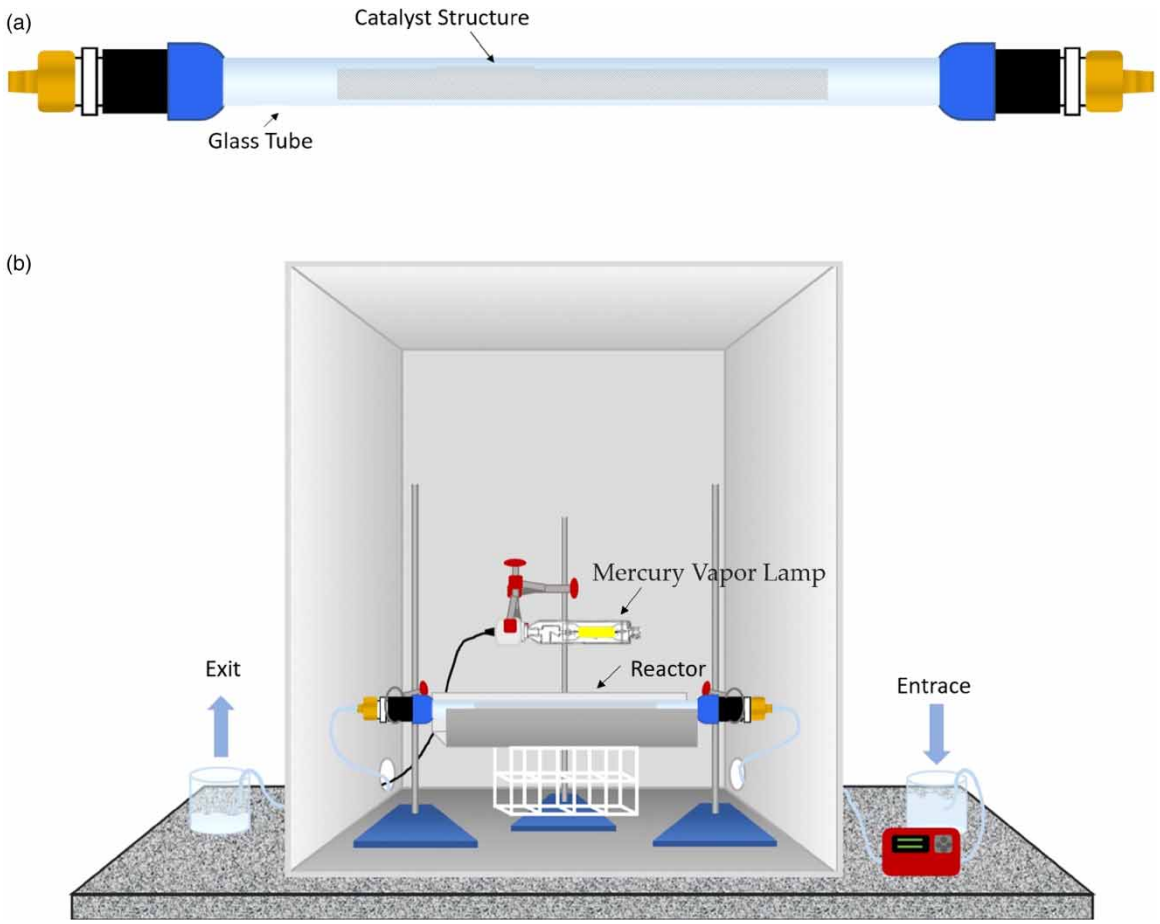

Figure 2 | (a) Photoreactor – structured catalyst and (b) continuous system.

A peristaltic pump was used to deliver the solution to the system. The concentrations of barium(II) and formic acid were the same for the batch tests. In addition to the flow, the effect of pH was also observed.

3. EXPERIMENTAL RESULTS

3.1. Powder catalysts

3.1.1. Batch tests

The batch tests were performed to verify the photocatalytic activity of the synthesized catalyst (TiO_2 sol–gel calcined at 823 K). First, the TiO_2 sol–gel catalyst was used in suspension (powder) form. In addition, it was compared to the commercial TiO_2 P25 catalyst. The results indicated that the synthesized sol–gel catalyst, despite having a slower rate of reaction, was able to remove barium(II) similar to the commercial one, as shown in Figure 3.

Fontana *et al.* (2018) carried out photocatalytic tests with different catalysts in suspension for the removal of barium(II). The approximate results for 90 min of reaction for the catalysts are as follows: commercial TiO_2, TiO_2 (Anatase), TiO_2 P25, and Nb_2O_5 were 6, 22, 30, and 34%, respectively.

Comparing the batch results, it is possible to see that the synthesized sol–gel catalyst behaves similar to the TiO_2 P25 and Nb_2O_5 catalysts in 90 min of reaction.

An adsorption reaction was also carried out under the same conditions as the photocatalytic reaction but in the absence of light. The results indicated that there was no adsorption on the catalyst surface, which is in agreement with Fontana *et al.* (2018). The literature describes the differences obtained for specific surface areas of catalysts due to preparation methods, calcination temperature, and addition of promoters (Ali *et al.* 2022a, 2022b; Fuziki

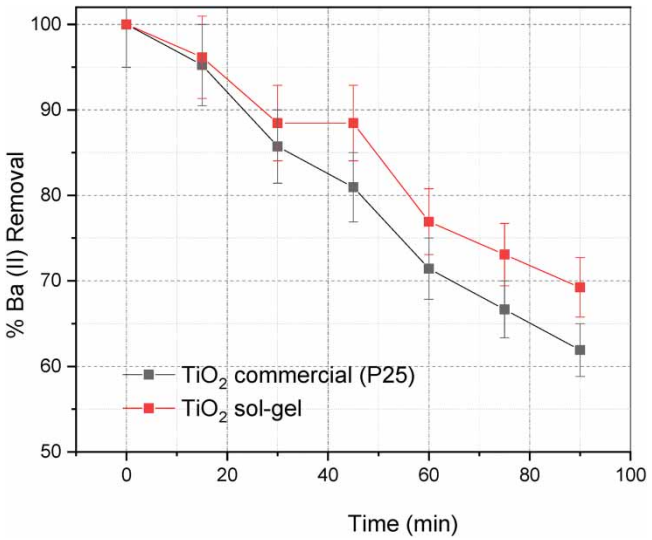

Figure 3 | Ba(II) ion removal from the synthetic solution in bath tests using the catalyst powder.

et al. 2023). In particular, TiO_2 prepared by the sol–gel method has higher values for surface area, 311 m^2/g, and commercial, 19.78 m^2/g (Lenzi *et al.* 2011).

3.2. Structured catalysts

The removal percentages of barium(II) ions in a continuous flow process for thin (TF), medium (TM), and thick (TG) nets calcined at three different temperatures (623, 823 and 1,023 K), under a constant flow rate of 1.5 mL/min, and reactional pH of 2.8 are shown in Figure 4.

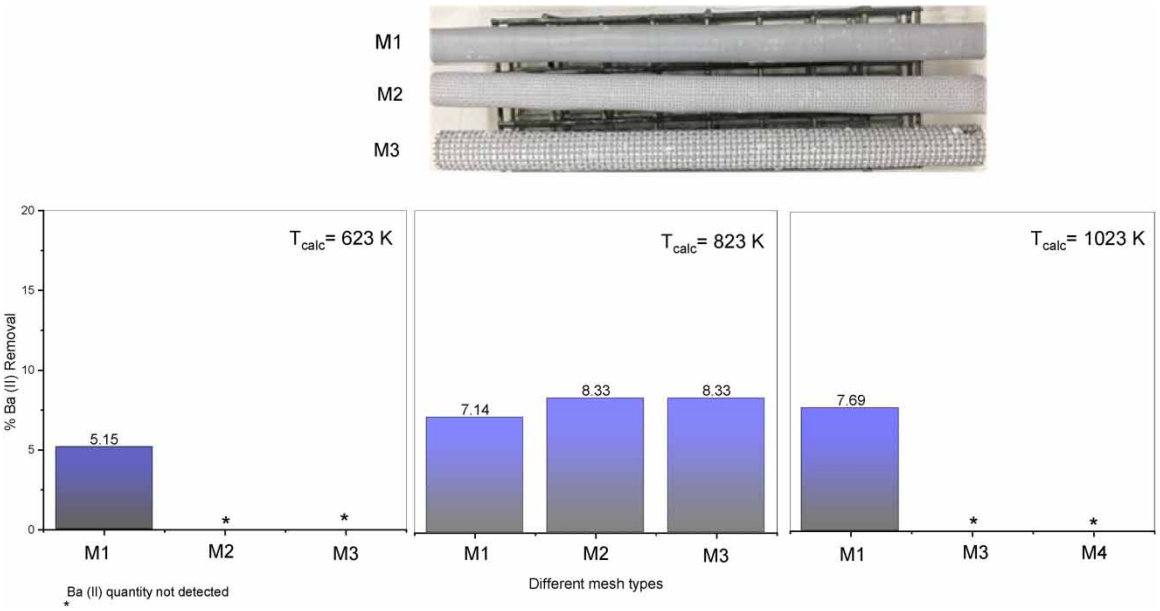

Figure 4 | Barium (II) removal results in a continuous flow [pH = 2.8; residence time 60 min].

At 623 and 1,023 K, barium(II) removal was seen only with the thin net (TF), and also this net immobilized more catalysts. On the other hand, TM and TG nets, both calcined at 623 and 1,023 K, did not remove Ba^{2+} ions, within the detection limit of the equipment. As shown by Denisov *et al.* (2017), the increase in temperature in the material generates more phase anatase in the structure, where the photoreactions are more efficient. However, throughout the reaction, it led to a more active stainless steel substrate component deposition on the

titanium dioxide film surface, obscuring the catalyst photocatalytic properties. Thus, higher calcination temperatures on structures like this are not as good as when using the catalyst in suspension. Also, Barati *et al.* (2009) got better results when calcined their catalysts at intermediary temperatures, nearby 823 K. Therefore, 823 K was the chosen temperature to carry out successive experiments, while the mesh considered for successive experiments was the medium one, TM, that came up with the same results as TG, but TM is lighter and malleable.

3.2.1. Effect of the flow rate and pH

From the results presented in Figure 4, the calcination temperature was set at 823 K and the mesh TM for the successive tests. For each run (Table 2), the pH and flow rate effect analysis were made by a simple experiment design, with two levels and triplicate on a central point – the last one for the eligibility of pure error – pH was changed so that the original pH value of the barium synthetic solution (2.8) remained within the chosen range for the experimental design levels, while the flow rate was lower to increase the residence time and, consequently, increase the contact of the solution with the catalyst. Table 2 shows the experimental design matrix.

Table 2 | Effect of experimental design, pH, and flow rate on the removal of barium(II) in a continuous flow process [$Ba^{2+} = 50\ g\ L^{-1}$]

Run	Flow rate (mL/min)	pH	Residence time (min)	Ba(II) removal (%)
1	1.08	3.8	83	8.82
2	1.44	6.0	63	20.83
3	1.08	3.8	83	9.52
4	0.72	6.0	125	20.00
5	1.44	1.5	63	10.00
6	0.72	1.5	125	10.53
7	1.08	3.8	83	11.43

In Figure 5, Pareto diagram, a *p*-test was made to observe the significant importance in a 95% confidence interval. As we can see, only the pH range was significantly important. Furthermore, Figure 5 indicates a significant curvature in the system, that is, it would be necessary to add axial points in order to form a central composite planning.

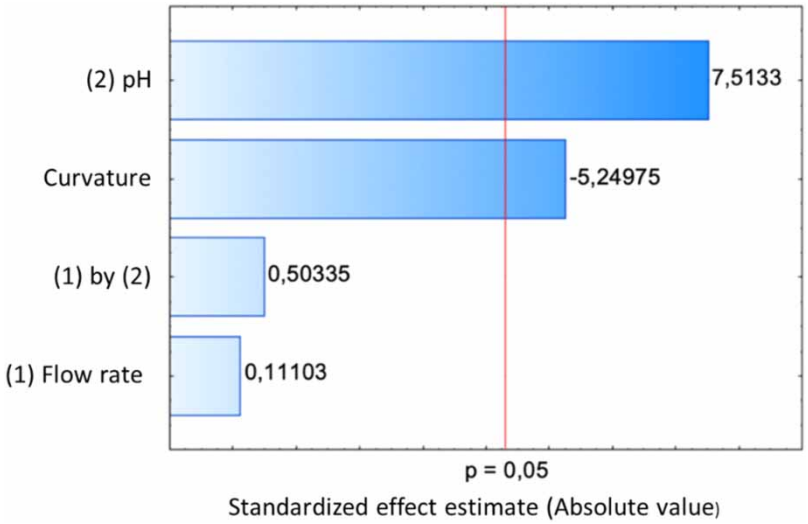

Figure 5 | Pareto chart of standardized effects [variable: % Ba(II) removal; seven runs; MS pure error = 1.825033].

As only pH had a significant effect, it was possible to analyze it separately. Thus, it was possible to observe that when increasing the level from −1 (1.5) to 1 (6.0), there was an increase of approximately 10% in the ion removal. In this way, basic solutions will provide higher barium(II) removal. So, before adding axial points to obtain a new design of experiments, it was made a solution pH displacement, as indicated in Table 3, for best results. The flow rate was kept constant, since within the analyzed gradient there was no significant effect on the results. To decode the variable, Equation (2) was used:

Table 3 | pH displacement matrix

Runs	Flow rate (mL/min)	Residence time (min)	x_{pH}	pH	Barium(II) removal (%)
1	1.08	83	0	3.8	9.93
2	1.08	83	1	6	11.11
3	1.08	83	2	8.2	15.79
4	1.18	82	3	10.4	11.76

$$\mathrm{pH} = [(\mathrm{pH}_1 - \mathrm{pH}_0) * x_{pH}] + \mathrm{pH}_0 \quad (2)$$

where pH_1 represents the pH value on level 1, pH_0 represents the pH value on level 0, and x_{pH} is the pH codified variable.

Thus, a new factorial experimental design on two levels was made at pH = 8.2 that presented a better result on the ion removal, and was chosen as the new central point. As seen before, the flow rate does not have a significant role in influencing the results, so it remained at the same previous levels and a new experimental design was generated (Table 4).

Table 4 | Effect of pH on the removal of barium(II) in a continuous flow process [$Ba^{2+} = 50\ gL^{-1}$]

Runs	Flow rate (mL/min)	pH	Residence time (min)	Ba(II) removal (%)
1	0.72	6.4	125	13.51
2	1.44	6.4	63	11.11
3	1.08	8.2	83	13.16
4	1.44	10	63	15.79
5	0.72	10	125	13.51
6	1.08	8.2	83	12.82
7	1.08	8.2	83	11.43

With the results from Table 5, a fresh analysis of the pH effects on the removal of barium(II) was conducted. Meanwhile, the Pareto diagram in Figure 6 indicates, through a *p*-test, that no factor had a significant effect on the test results within a 95% confidence interval.

Table 5 | Estimated effects of new pH levels on the removal of barium(II)

Factor	Effects (%)	Pure error	t(2)	p	Conf. limits −95%	Conf. limits +95%
Mean/interaction	13.48	0.458285	29.41402	0.001154	11.50816	15.45184
Curvature	−2.02	1.400083	−1.44277	0.285861	−8.04407	4.00407
(1) Flow rate (mL/min)	−0.06	0.91657	−0.06546	0.953761	−4.00368	3.88368
(2) pH	2.34	0.91657	2.553	0.125244	−1.60368	6.28368
(1) by (2)	2.34	0.91657	2.553	0.125244	−1.60368	6.28368

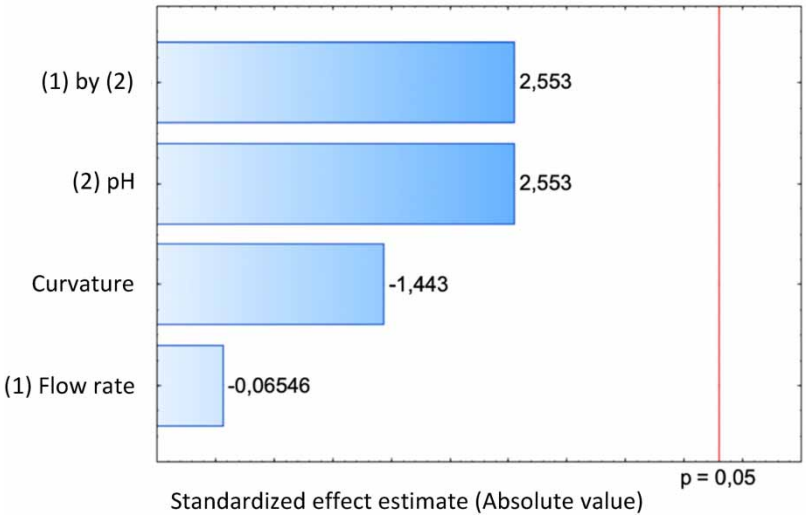

Figure 6 | Pareto chart of standardized effects for new pH levels [variable: % Ba(II) removal; seven runs; MS pure error = 0.8401].

Also, in these tests, the curvature did not present any significant effects, so it is not necessary to add axial points to make a PCC design. However, even with no significant effects in the chosen range for both pH and flow rate, analyzing the answers in Tables 3 and 4, it is possible to see that independent of volumetric flow rate, the system tends to have higher barium(II) removal when operating at more basic pH, as shown in Figure 7.

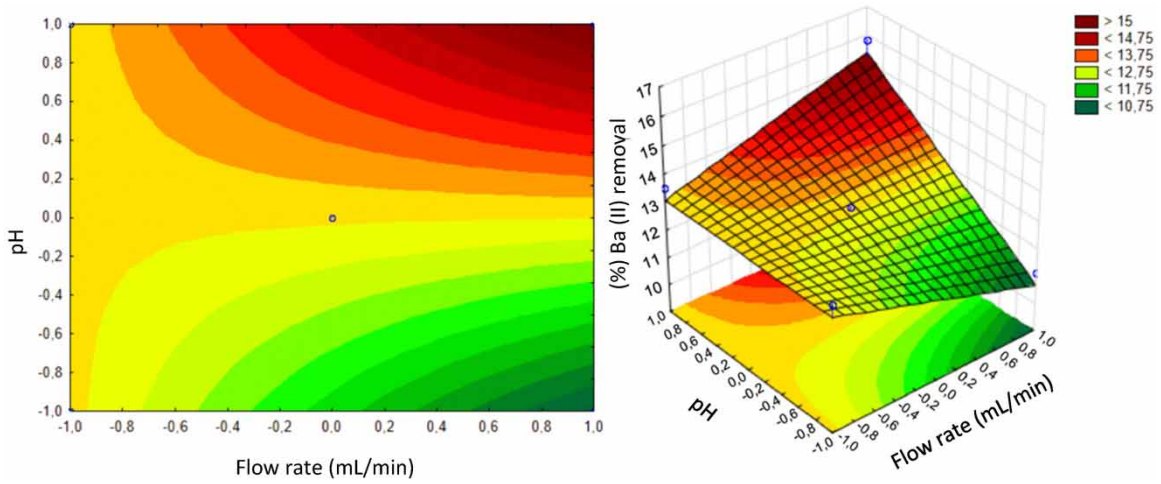

Figure 7 | Fitted surface from barium(II) removal in codify variables.

As shown by Majidnia & Idris (2015) and Fontana *et al.* (2018), barium(II) removal increases with pH increase to a certain extent, but increasing the solution pH beyond that did not provide any improvement. Chen & Ray (1998) discussed that although the high concentration of OH^- ions in the medium increases the electron promotion and the formation of positive holes, the carbon dioxide generated is trapped in the solution, resulting in the formation of bicarbonate and carbonate, which due to their high reaction constants with the hydroxyl radicals end up eliminating them. This may also explain why the pH variation in a range above 6 in these tests did not have a significant effect on barium(II) removal.

As higher pH levels did not have a significant impact on test answers, the best option is to use it in a neutral range, close to 7.0, because it does not require the addition of much reagent, saving resources.

About the flow rate, there was no evidence regarding its effect on the results. Thus, in this chosen gradient (level −1 to +1 or 0.72–1.44 mL/min), the flow variation has little impact on the response of the experiments.

However, the same cannot be said for much higher flow rates as the residence time would be very low, which would provide little contact between the element and catalyst. Meanwhile, in much lower flow rates, there would be an increase in the contact time with the catalyst. Although in this study there was no evidence of increase in barium(II) removal, instead the lower the flow rates, the lower was the ion removal. Perhaps by passing the solution very slowly through the reactor, it did not have enough movement to come into full contact with the catalyst, thus reducing the process efficiency.

3.3. Characterization

3.3.1. Point-of-zero charge (PZC)

The results of the zero charge point for the TiO_2 sol–gel catalyst are shown in Figure 8.

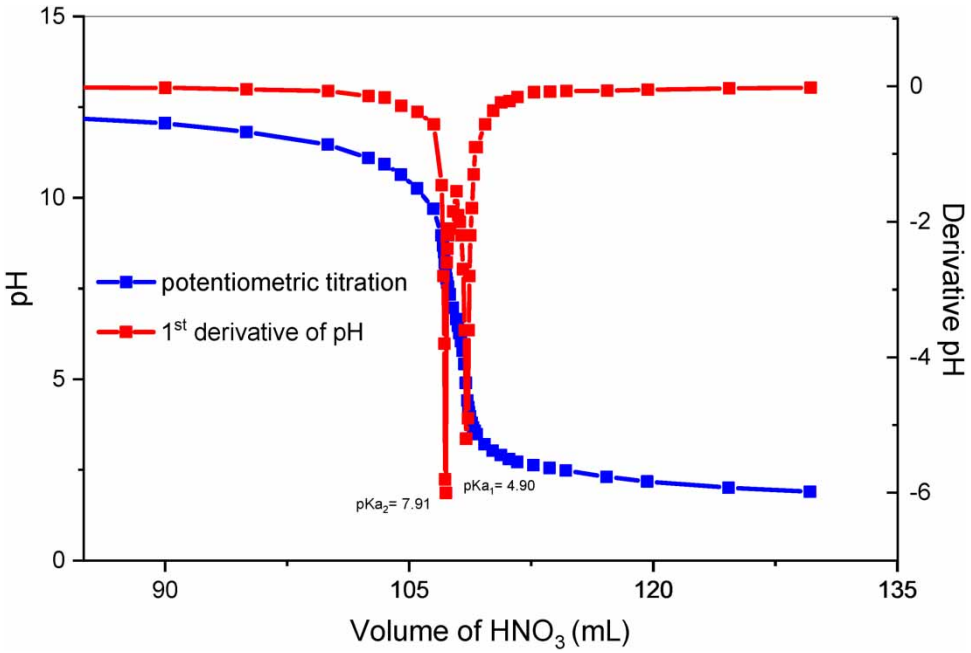

Figure 8 | pH changes in the photocatalyst suspension TiO_2 sol–gel vs. total volume of titrant and the derivative curve.

The corresponding pH values for Ka_1 and Ka_2 were 4.9 and 7.91, respectively. The pH_{PCZ} found for the catalyst synthesized was 6.4. This result was in agreement with the PCZ value found by Andronic *et al.* (2016) for titanium dioxide. Also, these results are close to the values found by other authors who used different analysis methods, such as the surface potential measurement by Chou & Liao (2005) or the zeta potential measurement (magnitude of repulsion or attraction of charges between particles) made by Arlos *et al.* (2016). Therefore, in the reaction medium with a pH lower than 6.4, the photocatalyst studied has a positively charged surface, generating affinity for molecules with a negative charge, while in the reaction medium with a pH greater than 6.4, the surface has a negative charge, thus having more affinity for positively charged molecules. This confirms and explains why the best degradation rates of the photocatalytic assays occurred at pH values above 6.0, since the barium molecules in the reaction medium have a positive charge (Ba^{2+}) and are, therefore, attracted to the catalyst surface when it is negatively charged, favoring the degradation process. Also, in media with low pH, there is a higher concentration of hydronium ions (H_3O^+) near the surface of the catalyst, producing repulsive forces and also compete with barium ions.

This behavior was observed by Majidnia & Idris (2015), who, when evaluating the effect of pH on the degradation of barium in radioactive wastewater using supported TiO_2 found that as the pH increased, the sorption capacity of Ba(II) increased steadily until reaching pH 8, but increasing the pH of the solution beyond this value did not show any improvement. Also, Fontana *et al.* (2018) had similar results when degrading barium using titanium dioxide as a photocatalyst in suspension, where the best degradation rates were observed at pH values greater than 7.

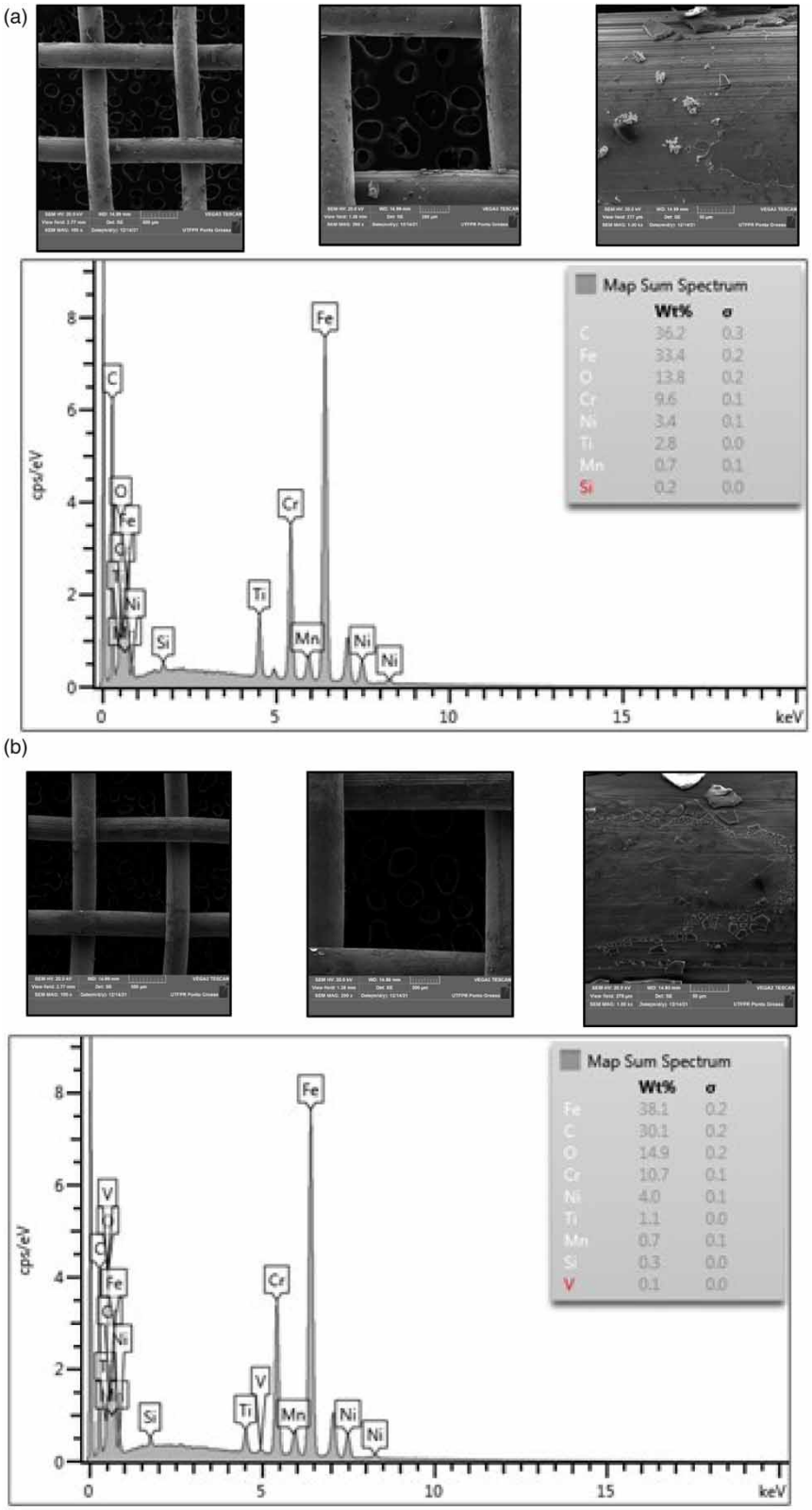

Figure 9 | MEV/EDS catalyst analysis: (a) before barium(II) removal and (b) after barium(II) removal.

However, both in the work by Majidnia & Idris (2015) similar to the work by Fontana *et al.* (2018), it was observed that at pH values higher than the PCZ of titanium dioxide, it did not obtain higher degradation rates, remaining constant or even lower. This effect was explained by Chen & Ray (1998), when they observed

in their experiment that the best pH value for degradation was close to the PCZ of TiO_2 because, despite the high concentration of OH^- ions in the medium, it increased the promotion of electrons and the formation of positive vacancies trapping the carbon dioxide generated in the solution, resulting in the formation of bicarbonate and carbonate, which due to their high reaction constants with hydroxyl radicals, end up eliminating them. This may also explain why the pH variation in a range above 6, in the tests carried out for the present work, did not show a significant effect on degradation.

3.3.2. SEM and EDS

An MEV/EDS analysis was made in order to verify the TiO_2 sol–gel catalyst surface adhesion on the nets (sample TM550), before (Figure 9(a)) and after (Figure 9(b)) the photocatalysis experiments. Thus, it is possible to see that there was catalyst adhesion, although not too much, something about 2.8%. On the other hand, after photocatalysis, the catalyst adhesion decreased to about 1.1%.

4. CONCLUSION

Comparing the results of the TiO_2 and P25 sol–gel catalysts in suspension, we observed that the synthesized catalyst is as efficient as the commercial catalyst (P25). When we use the continuous process, with the structured catalyst, there is a loss of activity due to the immobilization of the catalyst on the meshes, causing a decrease in active sites for the catalytic reaction to occur. In addition, effects of the calcination temperature of the meshes were observed. Calcination at 623 and 1,023 K causes a negative effect on the Ba(II) removal performance when stainless steel screens are used, in fine thick special meshes (TF and TG). On the other hand, at an intermediate temperature, 823 K, similar results were obtained for all mesh sizes (TF, TM, and TG), about 20.83% of Ba(II) removal at pH = 6.0 with residence time of 63 min in a continuous flow, which is a significant value compared to the removal of 24% of Ba(II) from the batch test at 63 min of reaction. The results obtained, under the conditions studied for pH, indicate that the best range is around 7, while the volumetric flow rate does not have a great effect on the removal of Ba^{2+} ions.

ACKNOWLEDGEMENTS

The authors are thankful to the Brazilian agencies CNPq and CAPES for financial support of this work, C^2MMa.

FUNDING

The authors declare that no funds, grants, or other support were received during the preparation of this manuscript.

AUTHOR CONTRIBUTIONS

All authors contributed to the study conception and design. Material preparation, data collection, and analysis were performed by L.N.B., G.G.L., A.M.T., E.A. and M.Z.F. The first draft of the manuscript was written by L.N.B., G.G.L., A.M.T., and M.Z.F. Also, the authors commented on previous versions of the manuscript. All authors read and approved the final manuscript.

DATA AVAILABILITY STATEMENT

All relevant data are included in the paper or its Supplementary Information.

CONFLICT OF INTEREST

The authors declare there is no conflict.

REFERENCES

Abbood, N. S., Ali, N. S., Khader, E. H., Majdi, H. S., Albayati, T. M. & Saady, N. M. C. 2023 Photocatalytic degradation of cefotaxime pharmaceutical compounds onto a modified nanocatalyst. *Res. Chem. Intermed.* **49**, 43–56. https://doi.org/10.1007/s11164-022-04879-3.

Abreu, E., Fidelis, M. Z., Fuziki, M. E., Malikoski, R. M., Mastsubara, M. C., Imada, R. E., Diaz de Tuesta, J. L., Gomes, H. T., Anziliero, M. D., Baldykowski, B., Dias, D. T. & Lenzi, G. G. 2021 Degradation of emerging contaminants: Effect of thermal treatment on Nb_2O_5 as photocatalyst. *J. Photochem. Photobiol. A Chem.* **419**, 113484. https://doi.org/10.1016/j.jphotochem.2021.113484.

Adamek, E., Baran, W., Ziemiańska-Błaszczyk, J. & Sobczak, A. 2019 Immobilisation of TiO_2-P25 on a glass fibre mat: Preparation, photocatalytic activity and stability. *Sol. Energy* **188**, 1232–1242. https://doi.org/10.1016/j.solener.2019.07.034.

Ali, N. S., Alismaeel, Z. T., Majdi, H. S., Salih, H. G., Abdulrahman, M. A., Cata Saady, N. M. & Albayati, T. M. 2022a Modification of SBA-15 mesoporous silica as an active heterogeneous catalyst for the hydroisomerization and hydrocracking of n-heptane. *Heliyon* **8**. https://doi.org/10.1016/j.heliyon.2022.e09737.

Ali, N. S., Kalash, K. R., Ahmed, A. N. & Albayati, T. M. 2022b Performance of a solar photocatalysis reactor as pretreatment for wastewater via UV, UV/TiO_2, and UV/H_2O_2 to control membrane fouling. *Sci. Rep.* **12**, 16782. https://doi.org/10.1038/s41598-022-20984-0.

Ali, N. S., Harharah, H. N., Salih, I. K., Cata Saady, N. M., Zendehboudi, S. & Albayati, T. M. 2023 Applying MCM-48 mesoporous material, equilibrium, isotherm, and mechanism for the effective adsorption of 4-nitroaniline from wastewater. *Sci. Rep.* **13**, 9837. https://doi.org/10.1038/s41598-023-37090-4.

Andronic, L., Isac, L., Miralles-Cuevas, S., Visa, M., Oller, I., Duta, A. & Malato, S. 2016 Pilot-plant evaluation of TiO_2 and TiO_2-based hybrid photocatalysts for solar treatment of polluted water. *J. Hazard. Mater.* **320**, 469–478. https://doi.org/10.1016/j.jhazmat.2016.08.013.

Arlos, M. J., Hatat-Fraile, M. M., Liang, R., Bragg, L. M., Zhou, N. Y., Andrews, S. A. & Servos, M. R. 2016 Photocatalytic decomposition of organic micropollutants using immobilized TiO_2 having different isoelectric points. *Water Res.* **101**, 351–361. https://doi.org/10.1016/j.watres.2016.05.073.

Atiyah, N. A., Albayati, T. M. & Atiya, M. A. 2022 Interaction behavior of curcumin encapsulated onto functionalized SBA-15 as an efficient carrier and release in drug delivery. *J. Mol. Struct.* **1260**, 132879. https://doi.org/10.1016/j.molstruc.2022.132879.

Barati, N., Sani, M. A. F., Ghasemi, H., Sadeghian, Z. & Mirhoseini, S. M. M. 2009 Preparation of uniform TiO_2 nanostructure film on 316l stainless steel by sol–gel dip coating. *Appl. Surf. Sci.* **255**, 8328–8333. https://doi.org/10.1016/j.apsusc.2009.05.048.

Bet-moushoul, E., Mansourpanah, Y., Farhadi, K. & Tabatabaei, M. 2016 TiO_2 nanocomposite based polymeric membranes: A review on performance improvement for various applications in chemical engineering processes. *Chem. Eng. J.* **283**, 29–46. https://doi.org/10.1016/j.cej.2015.06.124.

Bueno, I., He, H., Kinsley, A. C., Ziemann, S. J., Degn, L. R., Nault, A. J., Beaudoin, A. L., Singer, R. S., Wammer, K. H. & Arnold, W. A. 2023 Biodegradation, photolysis, and sorption of antibiotics in aquatic environments: A scoping review. *Sci. Total Environ.* **897**, 165301. https://doi.org/10.1016/j.scitotenv.2023.165301.

Chen, D. & Ray, A. K. 1998 Photodegradation kinetics of 4-nitrophenol in TiO_2 suspension. *Water Res.* **32**, 3223–3234. https://doi.org/10.1016/S0043-1354(98)00118-3.

Chou, J.-C. & Liao, L. P. 2005 Study on pH at the point of zero charge of TiO_2 pH ion-sensitive field effect transistor made by the sputtering method. *Thin Solid Films* **476**, 157–161. https://doi.org/10.1016/j.tsf.2004.09.061.

Cunha, D. L., Kuznetsov, A., Achete, C. A., Machado, A. E. d. H. & Marques, M. 2018 Immobilized TiO_2 on glass spheres applied to heterogeneous photocatalysis: Photoactivity, leaching and regeneration process. *PeerJ* **6**, e4464. https://doi.org/10.7717/peerj.4464.

Denisov, N. M., Baglov, A. V. & Borisenko, V. E. 2017 Role of iron and chromium in the photocatalytic activity of titanium dioxide films on stainless steel. *Inorg. Mater.* **53**, 176–180. https://doi.org/10.1134/S0020168517020030.

El-Kalliny, A. S., Ahmed, S. F., Rietveld, L. C. & Appel, P. W. 2014 Immobilized photocatalyst on stainless steel woven meshes assuring efficient light distribution in a solar reactor. *Drinking Water Eng. Sci.* **7**, 41–52.

Fidelis, M. Z., Abreu, E., Dos Santos, O. A. A., Chaves, E. S., Brackmann, R., Dias, D. T. & Lenzi, G. G. 2019 Experimental design and optimization of triclosan and 2.8-diclorodibenzeno-p-dioxina degradation by the Fe/Nb_2O_5/UV system. *Catalysts* **9**. https://doi.org/10.3390/catal9040343.

Fidelis, M., Favaro, Y. B., Santos, A. S. G. G. d., Pereira, M. F. R., Brackmann, R., Lenzi, G., Soares, O. S. G. P. & Andreo, O. A. B. 2023 Enhancing ibuprofen and 4-Isobutylacetophenone degradation: Exploiting the potential of Nb_2O_5 sol–gel catalysts in photocatalysis, catalytic ozonation, and photocatalytic ozonation. *J. Environ. Chem. Eng.*, 110690. https://doi.org/10.1016/j.jece.2023.110690.

Fontana, K. B., Lenzi, G. G., Seára, E. C. R. & Chaves, E. S. 2018 Comparision of photocatalysis and photolysis processes for arsenic oxidation in water. *Ecotoxicol. Environ. Saf.* **151**, 127–131. https://doi.org/10.1016/j.ecoenv.2018.01.001.

Fuziki, M. E. K., Ribas, L. S., Abreu, E., Fernandes, L., dos Santos, O. A. A., Brackmann, R., de Tuesta, J. L. D., Tusset, A. M. & Lenzi, G. G. 2023 N-Doped TiO_2-Nb_2O_5 Sol–Gel catalysts: Synthesis, characterization, adsorption capacity, photocatalytic and antioxidant activity. *Catalysts*. https://doi.org/10.3390/catal13091233.

Gar Alalm, M., Tawfik, A. & Ookawara, S. 2016 Enhancement of photocatalytic activity of TiO_2 by immobilization on activated carbon for degradation of pharmaceuticals. *J. Environ. Chem. Eng.* **4**, 1929–1937. https://doi.org/10.1016/j.jece.2016.03.023.

Graça, C. A. L., Ribeirinho-Soares, S., Abreu-Silva, J., Ramos, I. I., Ribeiro, A. R., Castro-Silva, S. M., Segundo, M. A., Manaia, C. M., Nunes, O. C. & Silva, A. M. T. 2020 A pilot study combining ultrafiltration with ozonation for the treatment of secondary urban wastewater: Organic micropollutants, microbial load and biological effects. *Water*. https://doi.org/10.3390/w12123458.

Guilarduci, V. V. d. S., Mesquita, J. P. d., Martelli, P. B. & Gorgulho, H. d. F. 2006 Adsorção de fenol sobre carvão ativado em meio alcalino. *Quim. Nova.* **29**, 1226–1232. https://doi.org/10.1590/S0100-40422006000600015.

Jabbar, N. M., Alardhi, S. M., Mohammed, A. K., Salih, I. K. & Albayati, T. M. 2022 Challenges in the implementation of bioremediation processes in petroleum-contaminated soils: A review. *Environ. Nanotechnol. Monit. Manage.* **18**, 100694. https://doi.org/10.1016/j.enmm.2022.100694.

Kadhum, S. T., Alkindi, G. Y. & Albayati, T. M. 2021 Determination of chemical oxygen demand for phenolic compounds from oil refinery wastewater implementing different methods. *Desalin. Water Treat.* **231**, 44–53. https://doi.org/10.5004/dwt.2021.27443.

Karaolia, P., Michael-Kordatou, I., Hapeshi, E., Drosou, C., Bertakis, Y., Christofilos, D., Armatas, G. S., Sygellou, L., Schwartz, T., Xekoukoulotakis, N. P. & Fatta-Kassinos, D. 2018 Removal of antibiotics, antibiotic-resistant bacteria and their associated genes by graphene-based TiO_2 composite photocatalysts under solar radiation in urban wastewaters. *Appl. Catal. B Environ.* **224**, 810–824. https://doi.org/10.1016/j.apcatb.2017.11.020.

Khadim, A. T., Albayati, T. M. & Cata Saady, N. M. 2022 Removal of sulfur compounds from real diesel fuel employing the encapsulated mesoporous material adsorbent Co/MCM-41 in a fixed-bed column. *Microporous Mesoporous Mater.* **341**, 112020. https://doi.org/10.1016/j.micromeso.2022.112020.

Kravchenko, J., Darrah, T. H., Miller, R. K., Lyerly, H. K. & Vengosh, A. 2014 A review of the health impacts of barium from natural and anthropogenic exposure. *Environ. Geochem. Health* **36**, 797–814. https://doi.org/10.1007/s10653-014-9622-7.

Lenzi, G. G., Fávero, C. V. B., Colpini, L. M. S., Bernabe, H., Baesso, M. L., Specchia, S. & Santos, O. A. A. 2011 Photocatalytic reduction of Hg(II) on TiO_2 and Ag/TiO_2 prepared by the sol–gel and impregnation methods. *Desalination* **270**, 241–247. https://doi.org/10.1016/j.desal.2010.11.051.

Lenzi, G. G., Abreu, E., Fuziki, M. E. K., Fidelis, M. Z., Brackmann, R., de Tuesta, J. L. D., Gomes, H. T. & dos Santos, O. A. A. 2022 17 α-Ethinylestradiol degradation in continuous process by photocatalysis using Ag/Nb_2O_5 immobilized in biopolymer as catalyst. *Top. Catal.* **65**, 1225–1234. https://doi.org/10.1007/s11244-022-01624-3.

Majidnia, Z. & Idris, A. 2015 Removal of barium from radioactive aqueous solution by PVA–alginate encapsulated titanium oxide using sunlight and other light types. *RSC Adv.* **5**, 63588–63595. https://doi.org/10.1039/C5RA01620G.

Manassero, A., Satuf, M. L. & Alfano, O. M. 2017 Photocatalytic reactors with suspended and immobilized TiO_2: Comparative efficiency evaluation. *Chem. Eng. J.* **326**, 29–36. https://doi.org/10.1016/j.cej.2017.05.087.

Martino, M. 2022 Structured supports and catalysts: Design, preparation, and applications. *Compounds*. https://doi.org/10.3390/compounds2030014.

Miranda-García, N., Maldonado, M. I., Coronado, J. M. & Malato, S. 2010 Degradation study of 15 emerging contaminants at low concentration by immobilized TiO_2 in a pilot plant. *Catal. Today* **151**, 107–113. https://doi.org/10.1016/j.cattod.2010.02.044.

Oliveira, J. R. P., Ribas, L. S., Napoli, J. S., Abreu, E., Diaz de Tuesta, J. L., Gomes, H. T., Tusset, A. M. & Lenzi, G. G. 2023 Green magnetic nanoparticles $CoFe_2O_4@Nb_5O_2$ applied in paracetamol removal. *Magnetochemistry*. https://doi.org/10.3390/magnetochemistry9080200.

Panniello, A., Curri, M. L., Diso, D., Licciulli, A., Locaputo, V., Agostiano, A., Comparelli, R. & Mascolo, G. 2012 Nanocrystalline TiO_2 based films onto fibers for photocatalytic degradation of organic dye in aqueous solution. *Appl. Catal. B Environ.* **121–122**, 190–197. https://doi.org/10.1016/j.apcatb.2012.03.019.

Pepe, F., de Gennaro, B., Aprea, P. & Caputo, D. 2013 Natural zeolites for heavy metals removal from aqueous solutions: Modeling of the fixed bed Ba^{2+}/Na^{+} ion-exchange process using a mixed phillipsite/chabazite-rich tuff. *Chem. Eng. J.* **219**, 37–42. https://doi.org/10.1016/j.cej.2012.12.075.

Rachel, A., Subrahmanyam, M. & Boule, P. 2002 Comparison of photocatalytic efficiencies of TiO_2 in suspended and immobilised form for the photocatalytic degradation of nitrobenzenesulfonic acids. *Appl. Catal. B Environ.* **37**, 301–308. https://doi.org/10.1016/S0926-3373(02)00007-3.

Shan, A. Y., Ghazi, T. I. M. & Rashid, S. A. 2010 Immobilisation of titanium dioxide onto supporting materials in heterogeneous photocatalysis: A review. *Appl. Catal. A Gen.* **389**, 1–8. https://doi.org/10.1016/j.apcata.2010.08.053.

Vaez, M., Moghaddam, A. Z., Mahmoodi, N. M. & Alijani, S. 2012 Decolorization and degradation of acid dye with immobilized titania nanoparticles. *Process Saf. Environ. Prot.* **90**, 56–64. https://doi.org/10.1016/j.psep.2011.07.005.

Zhang, H., Wang, Z., Li, R., Guo, J., Li, Y., Zhu, J. & Xie, X. 2017 Tio_2 supported on reed straw biochar as an adsorptive and photocatalytic composite for the efficient degradation of sulfamethoxazole in aqueous matrices. *Chemosphere* **185**, 351–360. https://doi.org/10.1016/j.chemosphere.2017.07.025.

Zhao, X., Pei, L., Zhang, Y.-N., Huang, H., Zheng, X., Liu, B. & Tong, M. 2022 Effective and irreversible removal of radioactive barium ions in MOF-808 framework functionalized sulfonic acid groups. *Green Chem. Eng.* **3**, 405–412. https://doi.org/10.1016/j.gce.2022.01.007.

First received 2 June 2023; accepted in revised form 25 September 2023. Available online 5 October 2023